3D inversion of time-lapse CSEM data for reservoir surveillance

Noel Black, Glenn A. Wilson, TechnoImaging, Alexander V. Gribenko and Michael S. Zhdanov, TechnoImaging and The University of Utah*

Summary

Recent studies have inferred the feasibility of time-lapse controlled-source electromagnetic (CSEM) methods for the surveillance of offshore oil and gas fields. However, quantitative interpretations have not been shown to ascertain what information about the reservoirs that may be recovered. We present a 3D inversion study of synthetic time-lapse CSEM data for the lateral water flooding of a reservoir unit where the hydrocarbon accumulation is trapped by a thin dome structure. We demonstrate that even with few constraints on the model, the flooding front can be recovered from 3D inversion. In this paper, synthetic time-lapse CSEM responses are simulated with the threshold about the noise floor and subject to multiple 3D inversion scenarios. The time-lapse CSEM inverse problem is highly constrained though inherently 3D since the geometry of the reservoir is established prior to production from high resolution seismic surveys; rock and fluid properties are measured from well logs; and multiple history matched production scenarios are contained in dynamic reservoir models.

Introduction

Decisions pertaining to reservoir management are made on the basis of dynamic reservoir simulations which attempt to characterize production and subsurface uncertainty from a suite of probable reservoir models populated with rock and fluid properties. These reservoir models are usually upscaled from detailed geological models built from geostatistical populations of well data within structural models inferred from seismic interpretation. During production, the confidence in a particular suite of reservoir models is garnered as the dynamic reservoir simulations are history matched with known volumetrics. Changes in rock and fluid properties manifest themselves as changes in acoustic impedance which, if measureable, can be interpreted from time-lapsed seismic surveys. These interpretations can further characterize the reservoir so as to reduce subsurface uncertainty (Walker et al., 2006). The sensitivity of seismic data to variations in fluid saturation is subtle, and it may only be after several years of production that a measurable change in acoustic impedance can be effectively interpreted. Should production veer towards the more unfavourable scenarios beforehand, the optimal intervention strategy can only be based upon reservoir models interpreted from the baseline seismic data. The basis of the various controlled-source electromagnetic (CSEM) methods is that their responses are sensitive to the lateral extents and thicknesses of resistive bodies embedded in conductive hosts. Hence, the initial applications have been for de-risking exploration and appraisal projects with direct hydrocarbon indication (Hesthammer et al., 2010). Reservoir surveillance is a logical extension of the CSEM method on the premise of fluid discrimination; in particular, tracking the position of the water contact. Recent model studies have implied the feasibility of time-lapse CSEM via 1D (Constable and Weiss, 2006), 2.5D (Orange et al., 2009) and 3D (Lien and Mannseth, 2008, Ziolowski et al., 2009; Black and Zhdanov, 2009) modeling. While these studies have qualitatively concluded that time-lapse CSEM responses are potentially measureable, none have yet conducted any 3D inversion for reservoir characterization. In this study, we do not conduct any dynamic reservoir modeling; instead we construct a series of 3D geoelectric models that correspond to static reservoir models at different production intervals (Figure 1). Hence, we avoid the need to implicitly construct a reservoir model containing rock physics relations that connect fluid saturations with electrical resistivity. The CSEM responses corresponding to these models are simulated and then subjected to multiple 3D inversion scenarios where data components and noise floors, water depth and a priori models are varied.

Model descriptions

Survey repeatability for time-lapse CSEM is subject to on-going research (e.g., Chuprin et al., 2008; Orange et al., 2009). We assumed that the tolerance of errors were less than the noise floor of a typical CSEM survey. Since the background conductivity model was assumed to be constant, the background fields were also constant. This meant that time-lapse CSEM responses were due entirely to the differences in anomalous fields resulting from different anomalous conductivity models. We modeled synthetic CSEM data for two different reservoir models; each being a thin dome and elliptical in shape with length 4 km along the major axis, and 3 km along the minor axis. The host was otherwise uniform with a resistivity of 1 Ωm. For the hydrocarbon-bearing reservoir units, we assumed a porosity of 30% and resistivity of 100 Ωm. We considered different scenarios where the recovery factors were 100% and 25%. In reality, recovery factors of 100% are never attained, although for high porosity gas fields, recovery factors greater than 80% are common. From Archie's Law, there is relatively little difference in the formation resistivities with either 80% or 100% water saturations. For oil fields, recovery factors between 25% and 50% are common with water injection. We should keep in mind however, that it is possible to inject water with lower resistivity which can

© 2010 SEG

offset the loss of resistivity contrast between water and hydrocarbon where only partial recovery is attainable. In all cases presented here, we assumed that the resistivities of the aquifer and any injected water were identical. The reservoirs were depleted primarily by lateral water flooding. We assumed that the reservoir was homogeneous during production; i.e., if inferred as an oil-bearing reservoir, pressure was maintained above bubble point so as to prevent formation of a gas cap.

CSEM data was simulated using the 3D integral equation method with inhomogeneous background conductivity (Zhdanov, 2009). The water depth was 350 m, and there was no bathymetry. For 100% recovery, the top of the reservoir structure is 1150 m below the sea floor. Figures 2, 3 and 4 show the inline and vertical electric fields, and transverse magnetic fields, respectively, measured over the field for an electric dipole source located at (0,0) km. In these figures, the horizontal location of the reservoir is outlined with a white ellipse that will be present in all modeling results. A white line is also drawn for the noise thresholds of 10^{-15} V/m and 10^{-10} nT/m for the electric and magnetic fields, respectively. For 25% recovery, the top of the reservoir structure was lowered to 1350 m below the sea floor. Figures 5, 6 and 7 show the inline and vertical electric fields, and transverse magnetic fields, respectively, measured over the field for an electric dipole source located at (0,0) km. In Figure 7, the noise threshold is plotted for 10^{-11} nT/m.

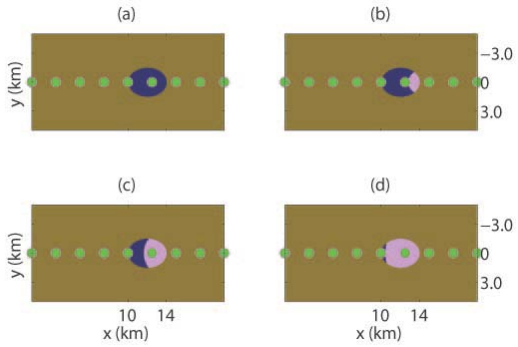

Figure 1. *Horizontal cross-section of the reservoir at 1490 m depth showing lateral flooding at different production intervals where hydrocarbon presence is shown in blue, and injected water is shown in pink; (a) pre-production, (b) ~25% production, (c) ~50% production and (d) ~90% production.*

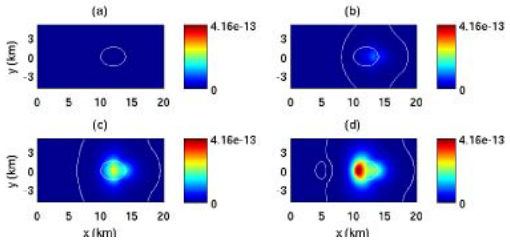

Figure 2. *Inline electric field differences relative to baseline at 0.08 Hz measured at the seafloor at four different production intervals with 100% recovery; (a) pre-production, (b) ~25% production, (c) ~50% production and (d) ~90% production. The reservoir outline is shown, as is the 10^{-15} V/m noise contour.*

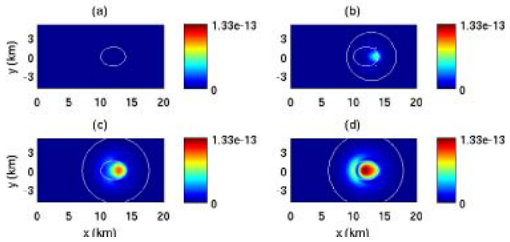

Figure 3. *Vertical electric field differences relative to baseline at 0.08 Hz measured at the seafloor at four different production intervals with 100% recovery; (a) pre-production, (b) ~25% production, (c) ~50% production and (d) ~90% production. The reservoir outline is shown, as is the 10^{-15} V/m noise contour.*

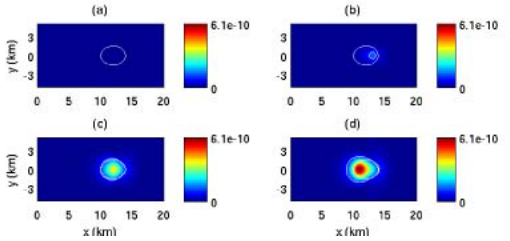

Figure 4. *Horizontal magnetic field differences relative to baseline at 0.08 Hz measured at the seafloor at four different production intervals with 100% recovery; (a) pre-production, (b) ~25% production, (c) ~50% production and (d) ~90% production. The reservoir outline is shown, as is the 10^{-10} nT/m noise contour.*

© 2010 SEG

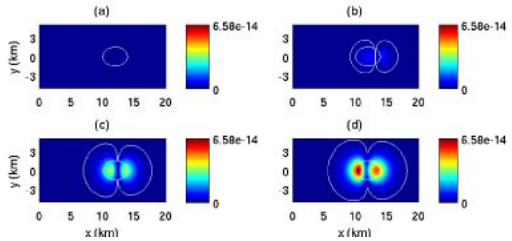

Figure 5. *Horizontal electric field differences relative to baseline at 0.08 Hz measured at the seafloor at four different production intervals with 25% recovery; (a) pre-production, (b) ~25% production, (c) ~50% production and (d) ~90% production. The reservoir outline is shown, as is the 10^{-15} V/m noise contour.*

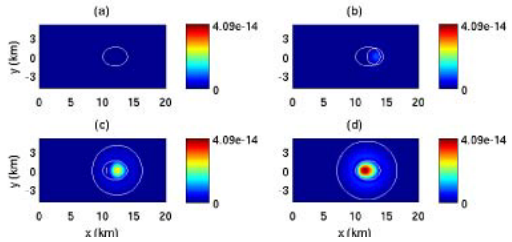

Figure 6. *Vertical electric field differences relative to baseline at 0.08 Hz measured at the seafloor at four different production intervals with 25% recovery; (a) pre-production, (b) ~25% production, (c) ~50% production and (d) ~90% production. The reservoir outline is shown, as is the 10^{-15} V/m noise contour.*

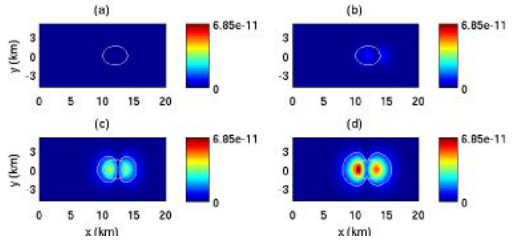

Figure 7. *Horizontal magnetic field differences relative to baseline at 0.08 Hz measured at the seafloor at four different production intervals with 25% recovery; (a) pre-production, (b) ~25% production, (c) ~50% production and (d) ~90% production. The reservoir outline is shown, as is the 10^{-10} nT/m noise contour.*

Inversion study

Modeling was based on the 3D integral equation method with inhomogeneous background conductivity for modeling. The inversion was iterated using the regularized re-weighted conjugate gradient (RRCG) method with focusing stabilizers (Zhdanov, 2002, 2009). In order to use the RRCG method for minimization of the Tikhonov parametric functional, it is necessary to calculate the sensitivities of the data with respect to the model parameters. We based our calculations of the Fréchet derivatives with those obtained using the quasi-analytical approximation with variable background. The details of these derivatives can be found in Gribenko and Zhdanov (2007). We applied 3D regularized inversion with focusing stabilizers. Traditional regularized inversions provide smooth solutions and thus have difficulties describing sharp boundaries between different geological formations. Focusing regularization makes it possible to recover subsurface models with sharper geoelectric contrasts and boundaries than can be obtained with smooth stabilizers (Zhdanov et al., 2010).

For the reservoir model at 1150 m below the sea floor, we simulated a CSEM survey that consists of 70 multi-component receivers distributed over orthogonal lines 1 km apart. CSEM data were simulated at 0.08, 0.125, 0.25, 0.5 and 0.75 Hz for a tow height 30 m above the seafloor and for transmitter-receiver offsets up to 8 km (Figure 8). The data were threshold above 10^{-15} V/m and 10^{-10} nT/m for the electric and magnetic fields, respectively. No noise was added to the CSEM data so we would not distort the effectiveness of inversion for recovering the position of the flooding front. All results are shown for the joint inversion of the inline and vertical electric field data, and transverse magnetic field data. There are two options for time-lapse CSEM inversion. One option is to invert the differences in CSEM responses. The other is to invert each CSEM response. We chose to demonstrate the latter in this paper. Figures 9, 10, and 11 show horizontal cross-sections of the reservoir units at different production intervals using the minimum support stabilizer. Figure 9 corresponds to the pre-production baseline survey. Figures 10 and 11 correspond to ~25% and ~50% production with 100% recovery. We can see that is possible to track the flooding front as a sharp boundary thanks to the use of focusing stabilizers.

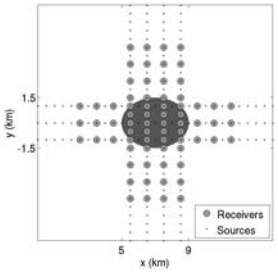

Figure 8. *3D marine CSEM survey and reservoir outline.*

© 2010 SEG

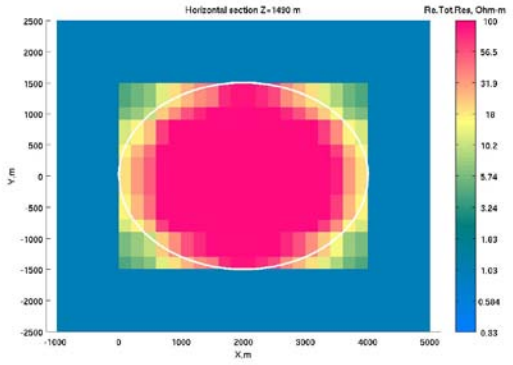

Figure 9. *Horizontal cross-section at 1490 m depth from 3D inversion of synthetic CSEM data prior to production. The reservoir outline is shown by the white line.*

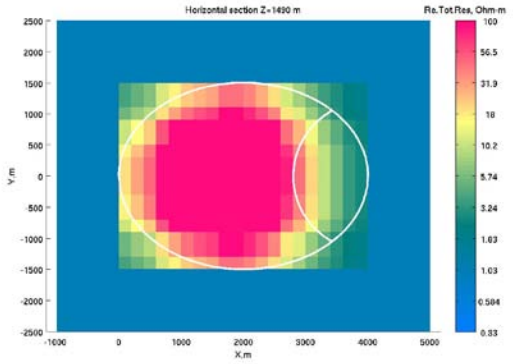

Figure 10. *Horizontal cross-section at 1490 m depth from 3D inversion of synthetic CSEM data measured for a partially depleted reservoir. The reservoir outline and oil-water contact is shown by the white line.*

Conclusions

The resistivity contrast across the flooding front means it is possible to monitor reservoirs using CSEM methods. In the models simulated here, the lateral flooding front was clearly identified in several field components. For the inline and vertical electric field components, the field differences are larger than the noise floors of the receivers, and are therefore expected to be detectable. However, this does not address questions regarding survey repeatability. Differences in the transverse magnetic field component are marginally detectable for a shallow reservoir with a perfect sweep production, and become undetectable for deeper reservoirs and more realistic recovery factors. Stacking the measured fields so as to increase the SNR by a factor of ten is sufficient for observability of the models studied here. The SNR decreases somewhat with increasing frequency, so for higher frequencies it is expected that more stacking will be necessary. The fact that time-lapse field differences do appear to be measureable at least for certain scenarios is promising.

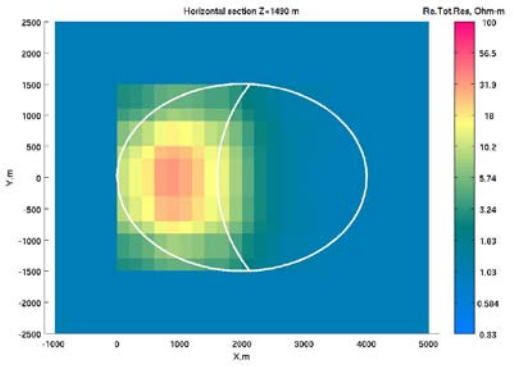

Figure 11. *Horizontal cross-section at 1490 m depth from 3D inversion of synthetic CSEM data measured for a partially depleted reservoir. The reservoir outline and oil-water contact is shown by the white line.*

While field maps may arguably provide a qualitative interpretation of the flooding front's position, inversion is required for quantitative interpretation so as to recover reservoir properties. Though time-lapse inversion is a highly constrained problem, we have demonstrated that it is possible to interpret the position of the flooding front in 3D with no a priori information. The use of constraints and/or a priori information will only improve the 3D inversion results. However, we note that it is essential to use focusing stabilizers so as to recover the sharp resistivity contrasts that exist across the flooding front rather.

Acknowledgements

Gribenko and Zhdanov acknowledge the support of The University of Utah's Consortium for Electromagnetic Modeling and Inversion (CEMI). The authors acknowledge TechnoImaging for permission to publish.

© 2010 SEG

EDITED REFERENCES

Note: This reference list is a copy-edited version of the reference list submitted by the author. Reference lists for the 2010 SEG Technical Program Expanded Abstracts have been copy edited so that references provided with the online metadata for each paper will achieve a high degree of linking to cited sources that appear on the Web.

REFERENCES

Black, N., and M. S. Zhdanov, 2009, Monitoring of hydrocarbon reservoirs using marine CSEM method: 79th Annual International Meeting, SEG, Expanded Abstracts, 850-853.

Chuprin, A., and D. Andreis, D., and L. MacGregor, 2008, Quantifying factors affecting repeatability in CSEM surveying for reservoir appraisal and monitoring: 78th Annual International Meeting, SEG, Expanded Abstracts, 648-651.

Constable, S., and C. J. Weiss, 2006, Mapping thin resistors and hydrocarbons with marine EM methods: Insights from 1D modeling: Geophysics, **71**, no. 2, G43–G51, doi:10.1190/1.2187748.

Hesthammer, J., A. Stefatos, M. Boulaenko, S. Fanavoll, and J. Danielsen, 2010, CSEM performance in light of well results: The Leading Edge, **29**, no. 1, 34–41, doi:10.1190/1.3284051.

Lien, M., and T. Mannseth, 2008, Sensitivity study of marine CSEM data for reservoir production monitoring: Geophysics, **73**, no. 4, F151–F163, doi:10.1190/1.2938512.

Orange, A., K. Key, and S. Constable, 2009, The feasibility of reservoir monitoring using time-lapse marine CSEM: Geophysics, **74**, no. 2, F21–F29, doi:10.1190/1.3059600.

Walker, G., P. Allan, T. Trythall, R. Parr, M. Marsh, R. Kjelstadi, O. Barkvad, D. Johnson, and S. Lane, 2006, Three case studies of progress in quantitative seismic-engineering integration: The Leading Edge, **25**, no. 9, 1161–1166, doi:10.1190/1.2349821.

Ziolkowski, A. M., R. Parr, D. Wright, and V. Nockles, 2009, Multi-transient EM repeatability experiment over Harding field: Presented at the 71st EAGE Conference and Exhibition.

Zhdanov, M. S., 2002, Geophysical Inverse Theory and Regularization Problems: Elsevier.

Zhdanov, M. S., 2009, Geophysical Electromagnetic Theory and Methods: Elsevier.

Zhdanov, M. S., E. P. Velikhov, M. Cuma, G. Wilson, N. Black, and A. Gribenko, 2010, Exploring multiple inversion scenarios for enhanced interpretation of CSEM data – An iterative migration analysis of the Shtokman gas field: First Break, **28**, 95–101.

© 2010 SEG